Molecular Basis of Prostaglandin E_2 Reuptake by Organic Anion Transporter PGT

Zhini Zhu[1#], Yaohui Li[1#*], Hao Xia[2#], Chuanhui Yang[1#], Zixuan Zhou[1#], Yulin Chao[1], Qian Ba[3*], Dianfan Li[2,4,*], Qianhui Qu[1*]

[1]Eye & ENT Hospital, Institutes of Biomedical Sciences，Department of Systems Biology for Medicine, Shanghai Key Laboratory of Medical Epigenetics, Fudan University, Shanghai, China.

[2]State Key Laboratory of Molecular Biology, CAS Center for Excellence in Molecular Cell Science, Shanghai Institute of Biochemistry and Cell Biology, University of CAS, Chinese Academy of Sciences (CAS), Shanghai, China.

[3]Laboratory Center, Shanghai Municipal Hospital of Traditional Chinese Medicine, Shanghai University of Traditional Chinese Medicine, Shanghai, China

[4]School of Agriculture and Biotechnology, Sun Yat-Sen University, Shenzhen, China

[#] These authors contributed equally

Correspondence: qqh@fudan.edu.cn; dianfan.li@sibcb.ac.cn; qba@shsmu.edu.cn; lvhailiyaohui@163.com

Supplementary Figures 1-16

Supplementary Tables 1-2

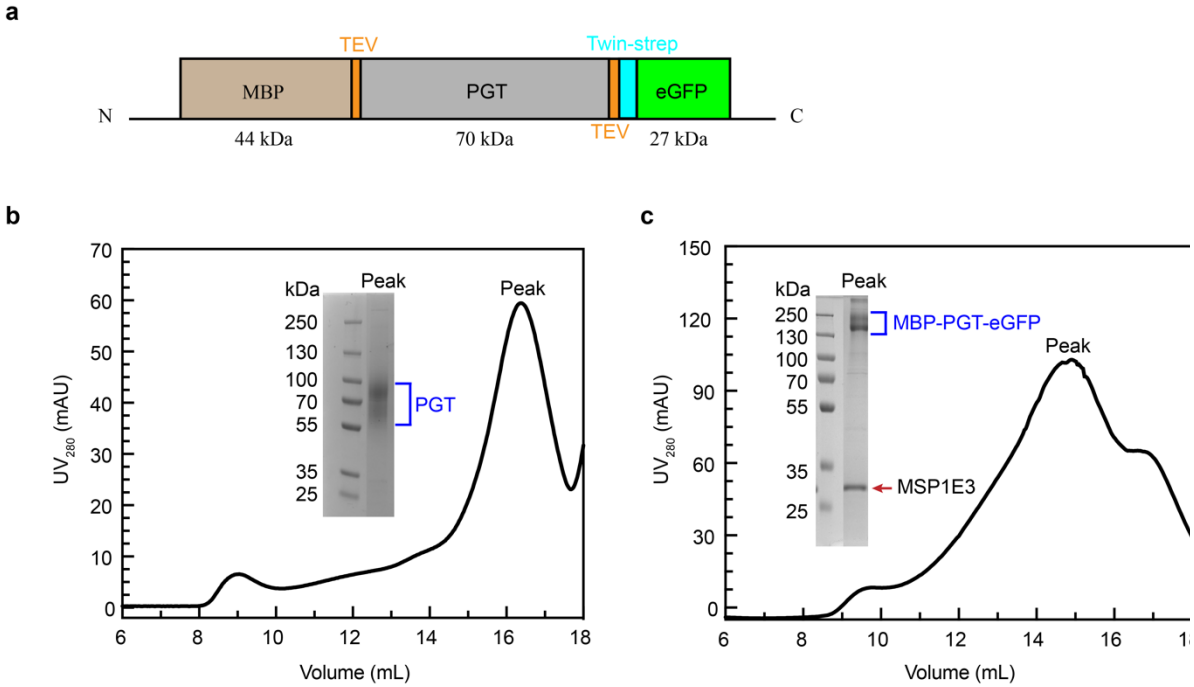

Supplementary Figure 1. PGT protein purification in detergent and in nanodisc. a, Schematic of PGT construct. MBP fusion was utilized to improve protein expression, and eGFP was tagged to track the purification process. **b** and **c**, Size exclusion chromatography profiles (SEC) and SDS-PAGE results (inset) of PGT protein prepared in detergent micelles (**b**) and in lipid nanodiscs (**c**), respectively.

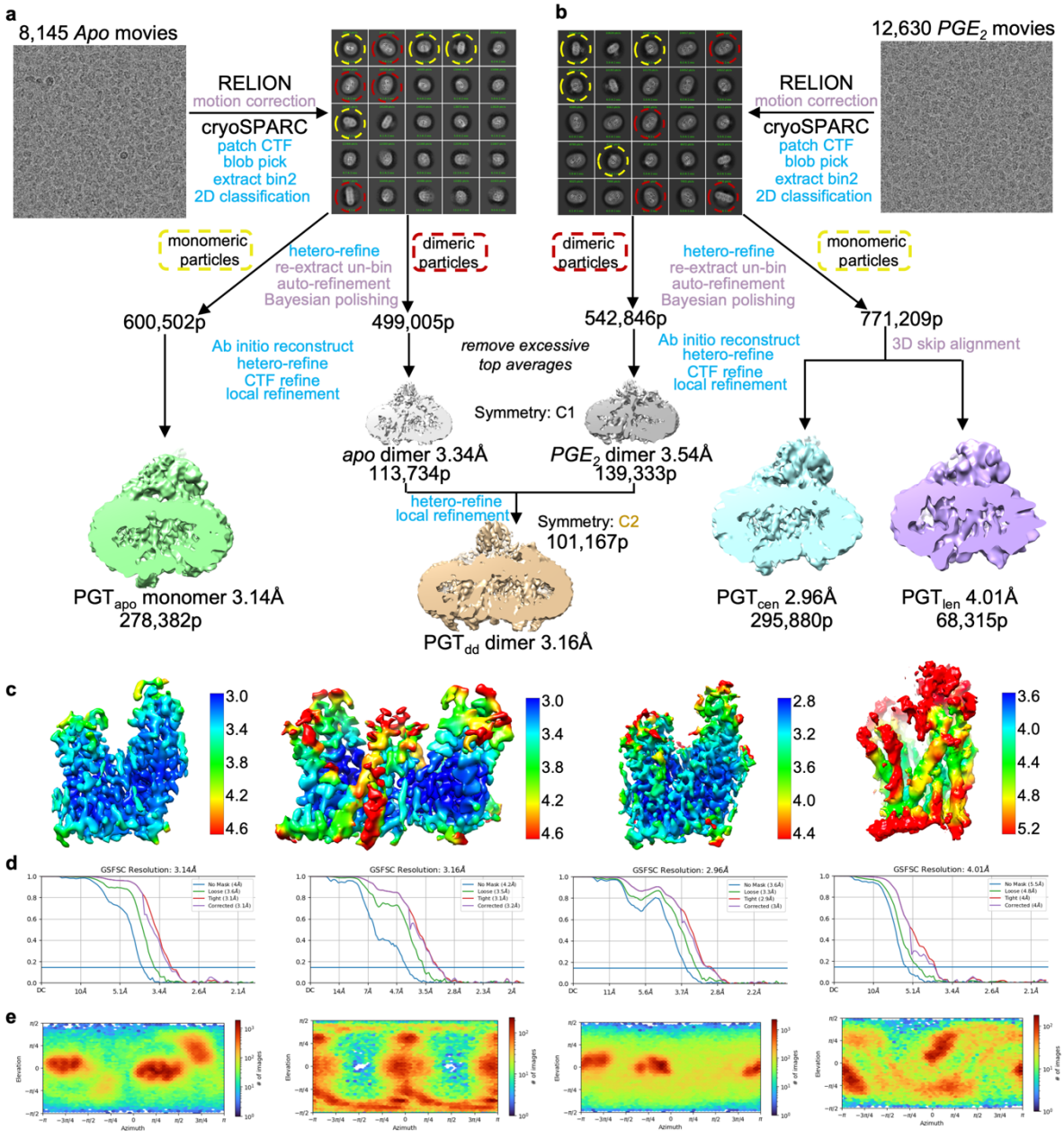

Supplementary Figure 2. Cryo-EM analysis of PGT apo and PGE_2-bound samples in detergent. **a** and **b**, Processing workflow for apo and PGE_2 data. Representative raw images and 2D class averages are shown. Monomeric and dimeric particles are pooled and processed separately. The final higher-resolution map of PGT dimer is reconstructed from combined apo and PGE_2 dimeric particles, as the two maps are nearly identical. **c,** Sideview of local resolution distribution for apo, dimer, PGE_2-bound at central site (PGT_{cen}) and PGE_2-bound close to lateral entry (PGT_{len}) sharpened maps, respectively. **d,** Resolution estimated by the gold-standard Fourier shell correlation (GSFSC) with cutoff at 0.143. **e,** Angular distribution heatmap of the final particles in corresponding map reconstructions.

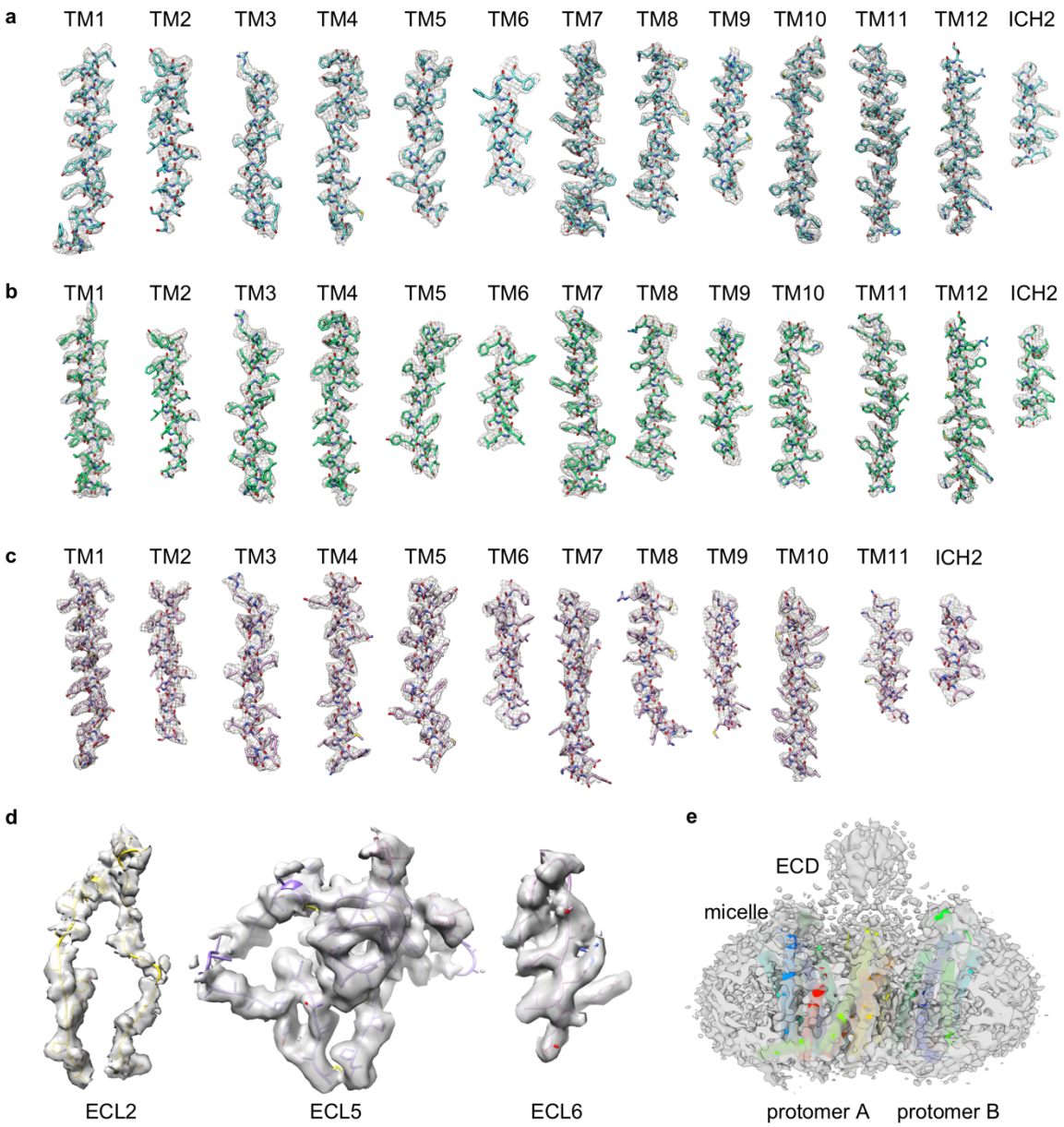

Supplementary Figure 3. Cryo-EM density for PGT_{apo}, PGT_{cen} and PGT_{dd} structures. a-c, Density corresponding to representative helices of PGT_{apo} (**a**), PGT_{cen} (**b**), and PGT_{dd} (**c**). **d,** The fitting of ECL2, ECL5 and ECL6 into the density in the PGT_{apo} map. **e,** The PGT_{dd} dimer map showing well-resolved densities for the transmembrane region and featureless density for the ECD region.

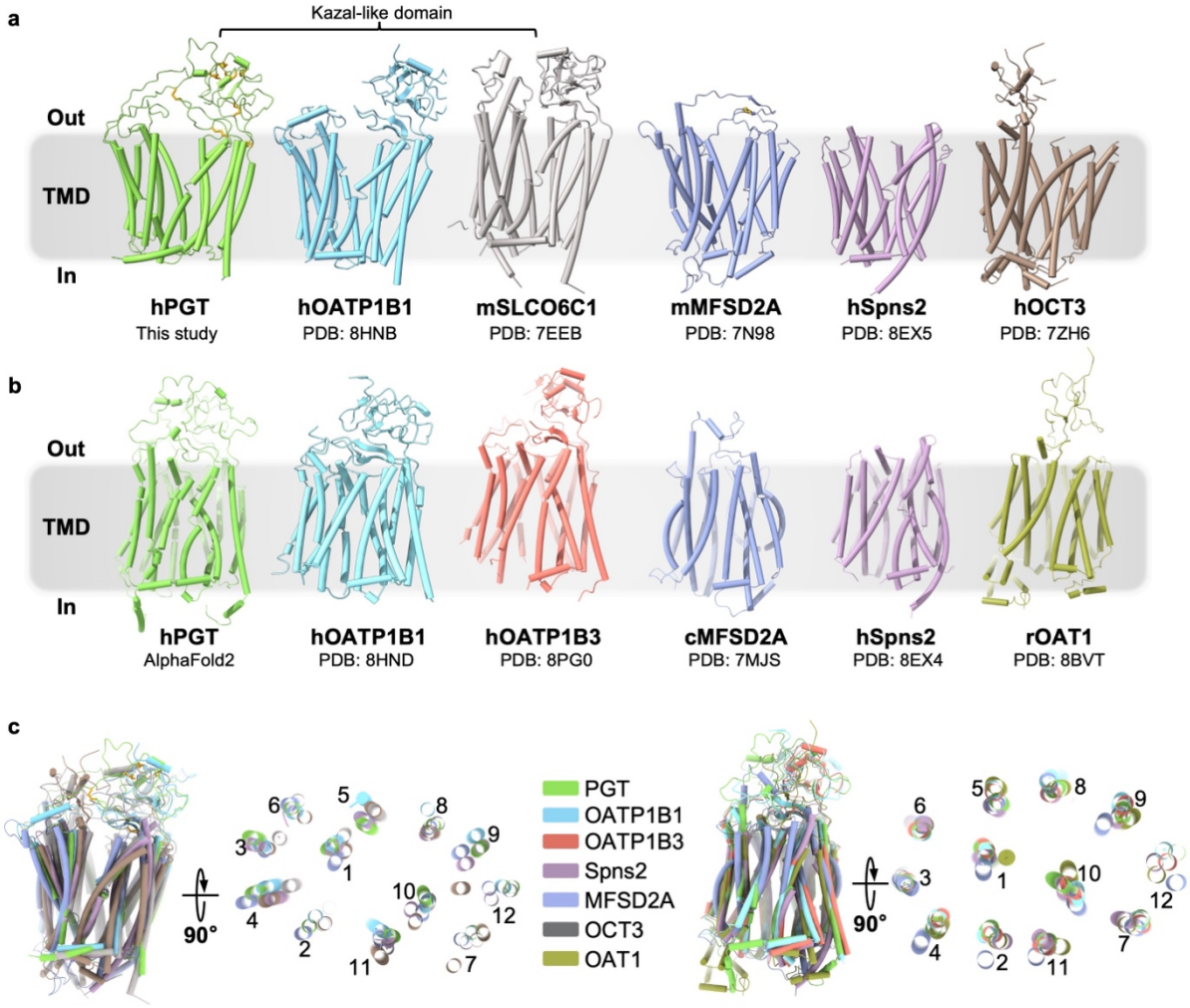

Supplementary Figure 4. Comparison between PGT and other lipid-like ligand MFS transporters.

a, Structures of the outward-facing human PGT (transport prostaglandins, this study), human OATP1B1 (transport metabolites and drugs, PDB: 8HNB), mouse SLCO6C1 (unknown substrate, PDB: 7EEB), mouse MFSD2A (transport lysophosphalipids, PDB: 7N98), human Spns2 (transport sphingosine-1-phosphate, PDB:8EX5), and human OCT3 (transport organic cation ligands, PDB: 7ZH6). PGT, OATP1B1 and SLCO6C1 belong to the same SLCO family that contains a conserved extracellular Kazal-like domain, rich in intra- and inter-loop disulfide bonds. In contrast, only MFSD2A contains one inter-loop disulfide bond in this region. **b,** Architectures of the inward-facing PGT (AlphaFold2 model), human OATP1B1 (PDB: 8HND), human OATP1B3 (transport metabolites and drugs as OATP1B1, PDB: 8PG0), chicken MFSD2A (PDB: 7MJS), human Spns2 (PDB: 8EX4), and rat OAT1 (transport organic anion ligands, PDB: 8BVT). Aside from the shared MFS transport domain similarity, PGT exhibits a large distinctive ECD which features eight. **c,** Structural alignment of the outward-facing conformations of these transporters, with Ca root mean square deviation (RMSD) within 1.1 Å. On the right, the inward-facing conformations are compared among the transporters listed.

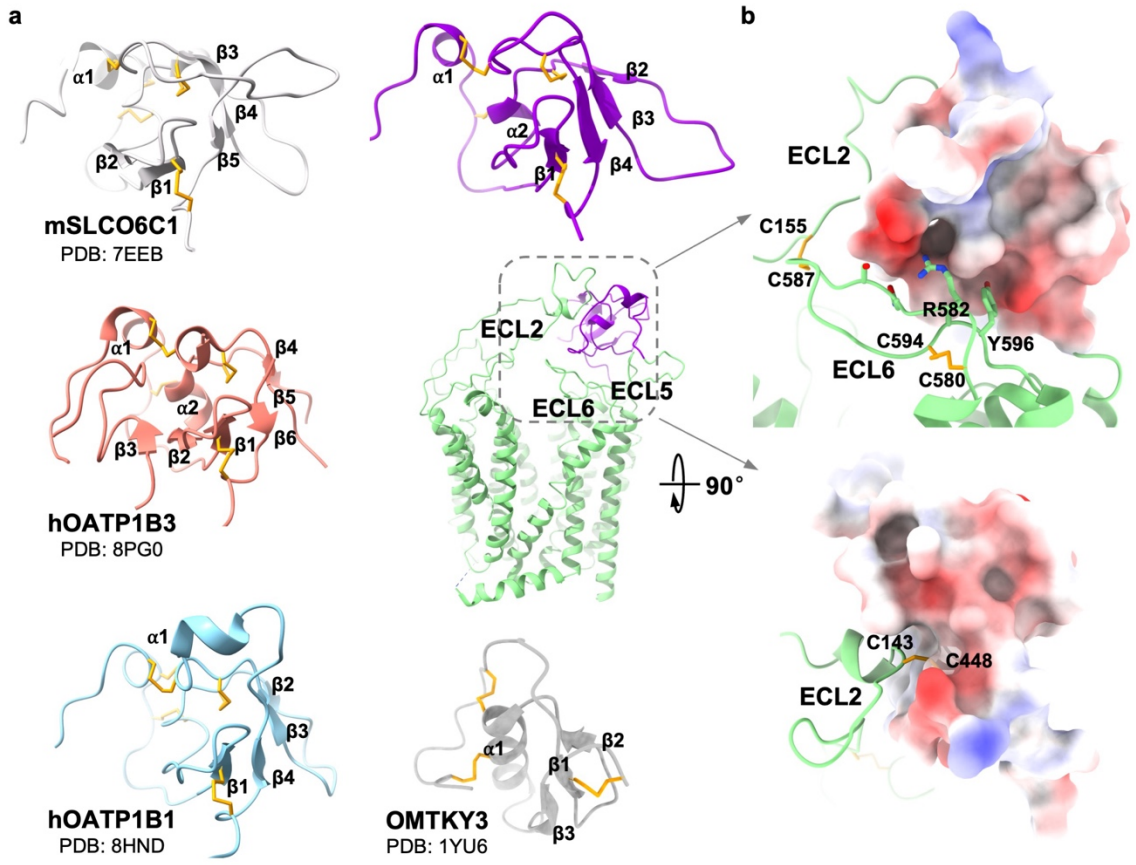

Supplementary Figure 5. PGT Kazal-like domain centers the ECD interaction network. a, The Kazal-like domains from human PGT/SLCO2A1/OATP2A1 (this study), mouse SLCO6C1 (PDB: 7EEB), human OATP1B3 (PDB: 8PG0), human OATP1B1 (PDB: 8HND), and the proteinase inhibitor turkey ovomucoid protein OMTKY3 domain (PDB: 1YU6) are shown in ribbon. The anti-parallel b-sheet and short a-helices are labelled. Disulfide bonds are shown in orange sticks. **b**, Detailed interactions between the PGT Kazal-like domain and ECL6 (top) or ECL2 (bottom). ECL2 and ECL6 are shown as ribbons, with key residues in sticks representations. The electrostatic potential surface of Kazal-like domain is presented.

a

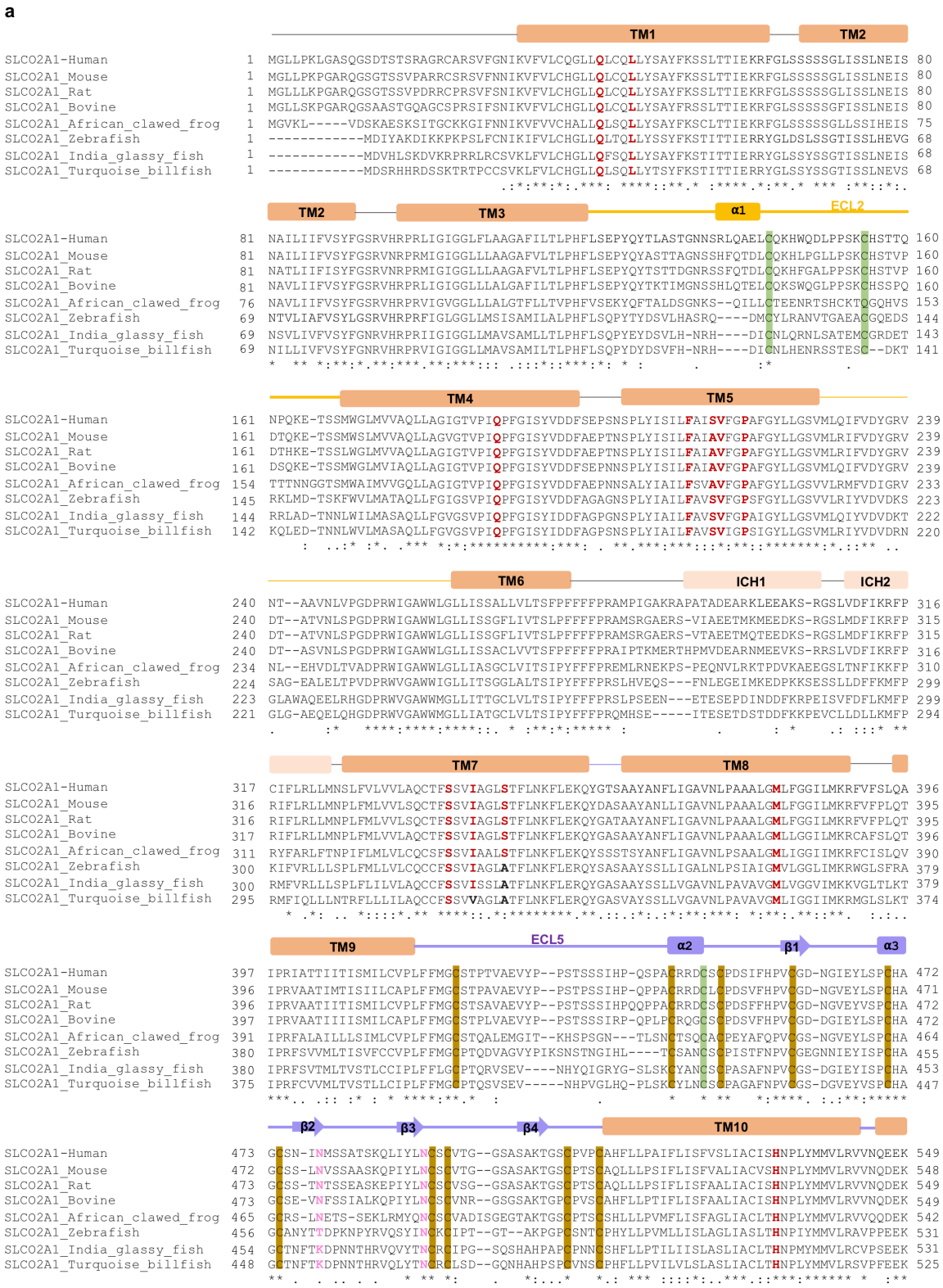

See next page for caption

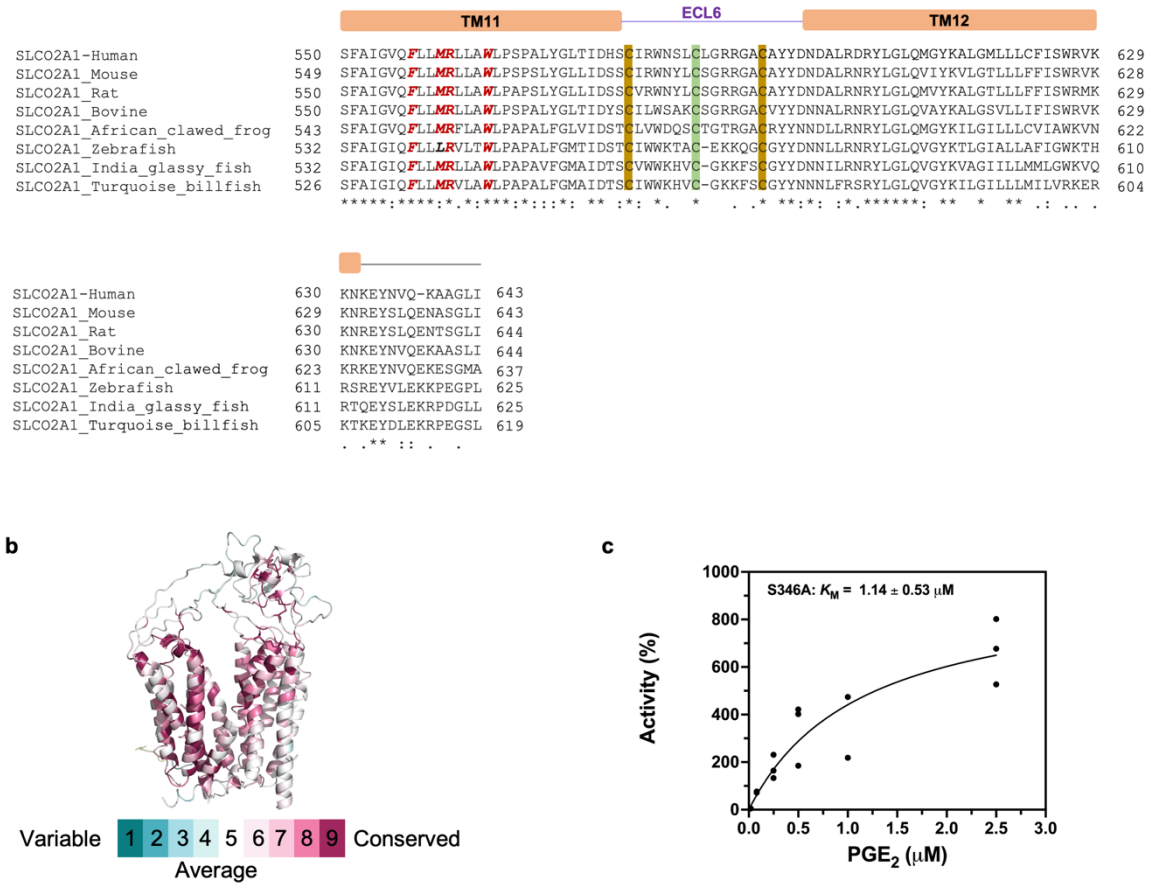

Supplementary Figure 6. Sequence conservation of PGT/SLCO2A1 orthologs. a, Sequence alignment of PGT/SLCO2A1 from human, mouse, rat, bovine, African clawed frog, zebrafish, India glassy fish and Turquoise billfish. Asterisk, colon, and dot indicate identical, conserved, and semi-conserved substitutions, respectively. Secondary structure segments of PGT/SLCO2A1 shown above are in accordance with Figure 1b. Cysteines forming inter-domain disulfide bonds (green) and intra-domain disulfide bonds (tan) are highlighted. Residues involved in PGE_2 binding are colored red. The ECL5 segment for the conserved Kazal-like domain between TM9 -TM10 is indicated with purple coloring on the top. N-glycosylation sites are colored pink. **b,** Amino acid conservation among the PGT/SLCO2A1 orthologs is mapped onto the PGT structure. **c,** Transport kinetics analysis of S346A mutant.

See next page for caption

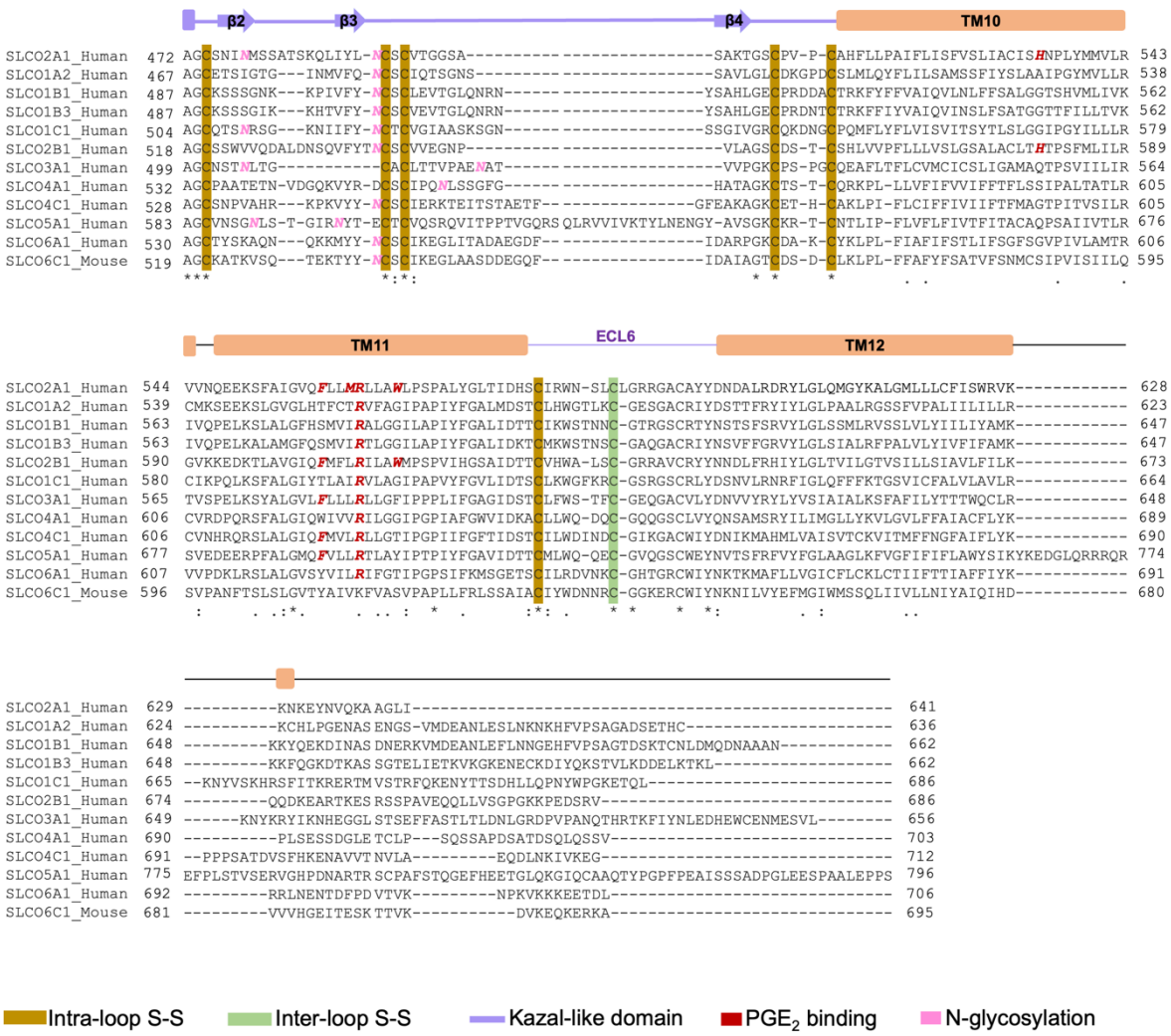

Supplementary Figure 7. Sequence alignment of human SLCO family members. Sequences of the 11 human SLCO family members and mouse sperm-specific SLCO6C1 are aligned. The secondary structure of PGT/SLCO2A1 is shown above. All sites are colored as in Supplementary Figure 6.

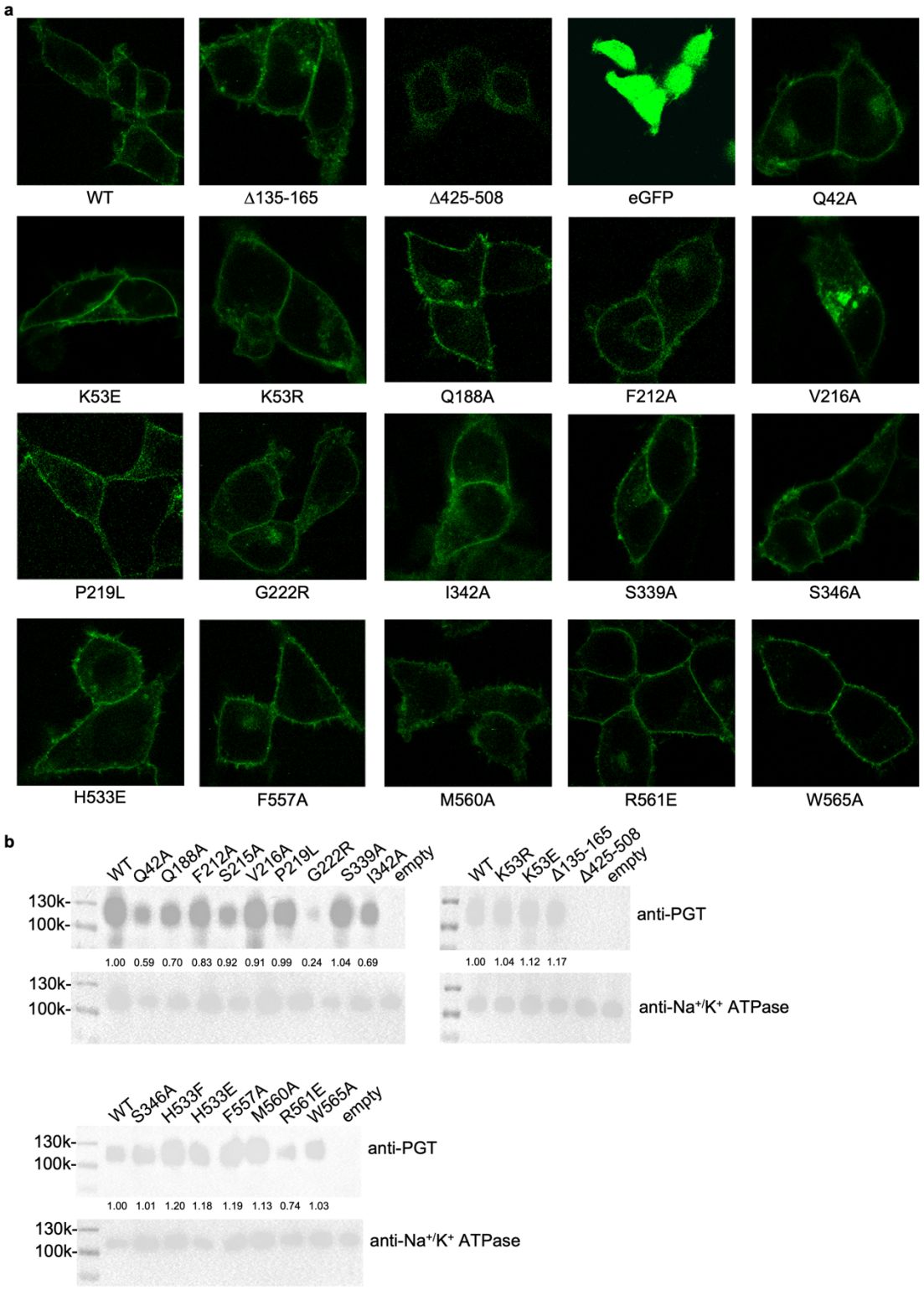

Supplementary Figure 8. Expression and localization of PGT WT and mutants in stable HEK293T cells. a, PGT constructs are tagged with eGFP for visualization in stably transfected HEK293T cells. Confocal microscopy analysis showed that most mutants localize correctly to cell surface as WT PGT, except the Δ425-508 mutant which mainly form puncta accumulated in cytoplasm. Cells transfected with eGFP alone are used for control. **b,** Surface expression levels of WT and mutants measured by biotinylation. The representative factors calculated based on the integrated band intensity are indicated in each lane. Cell surface transmembrane protein Na^+/K^+-ATPase is used as loading control.

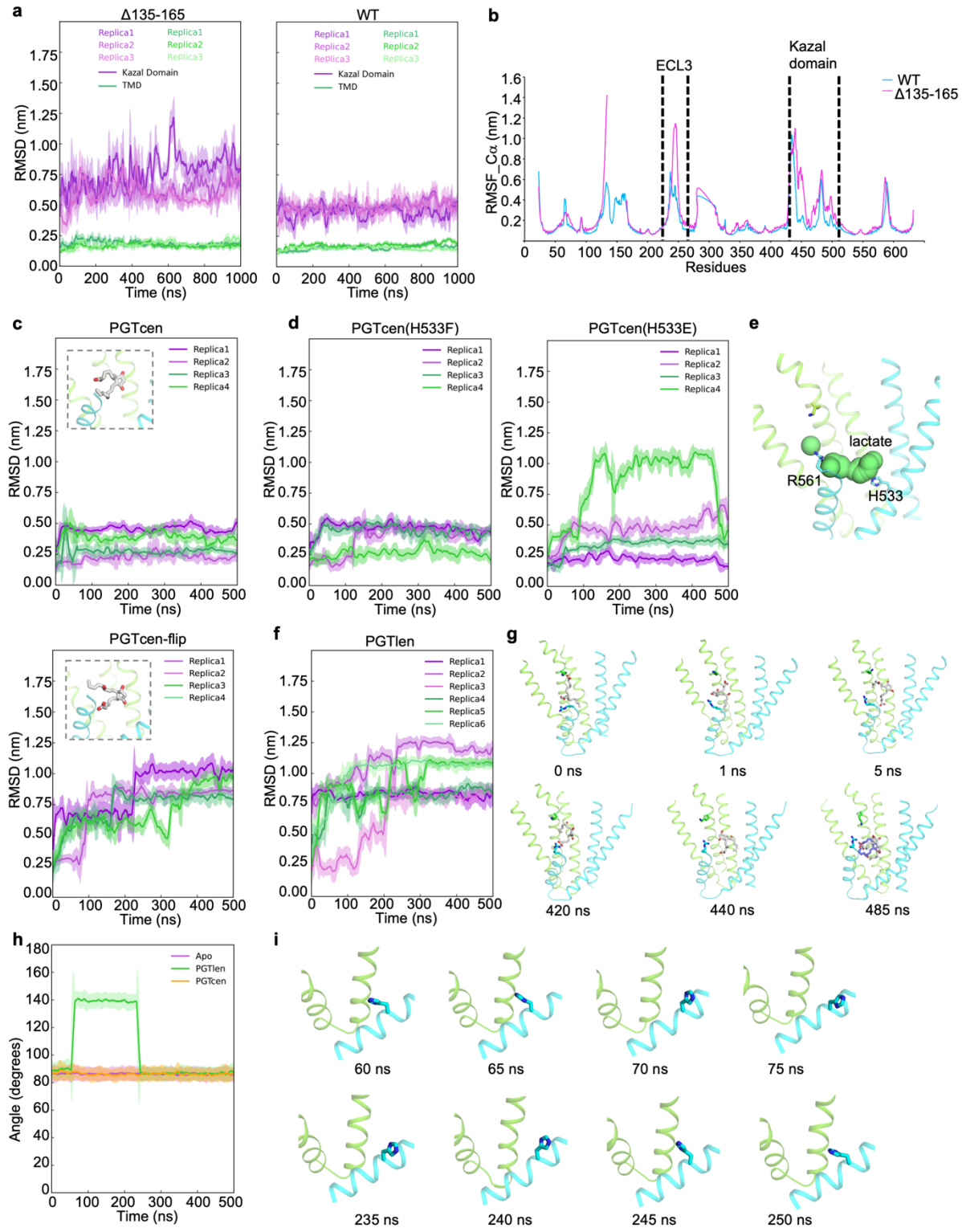

Supplementary Figure 9. Molecular dynamics simulation analysis. a, Root mean square deviation (RMSD) plots of MD simulations for WT PGT and $PGT_{\Delta 135\text{-}165}$. Simulation traces from three simulations are shown. Purple, the Kazal-like domain; green, the TMD. **b,** Root mean square fluctuation (RMSF) of Cα positions are plotted for WT PGT (blue) and $PGT_{\Delta 135\text{-}165}$ (purple). The average of triplicate runs is shown. **c,** MD simulation trajectories of PGE_2 in the PGT_{cen} state (top panel), and the upside-down flipped PGE_2 pose as control (bottom panel). **d,** MD simulations of PGE_2 in the PGT_{cen} state with either H533F (left) or H533E (right) mutation. **e,** Docking analysis of lactate (green balls) at PGT central

binding site. Two frequent lactate binding residues (His533 and Arg561) were highlighted in sticks. **f,** MD simulation trajectories of PGE_2 in the PGT_{len} state. **g**, Representative snapshots in one simulation trajectory showing transition of PGT_{len} pose (grey sticks) to a PGT_{cen}-like configuration (purple sticks, at frame 485ns). **h**, His533 orientations in Apo, PGT_{len} and PGT_{cen} states during MD simulations. The dihedral angle of His533 side chain relative to its main chain was calculated as an approximate metric for orientation index. **i**, Representative snapshots of His533 conformational dynamics in one PGT_{len} MD simulation trajectory.

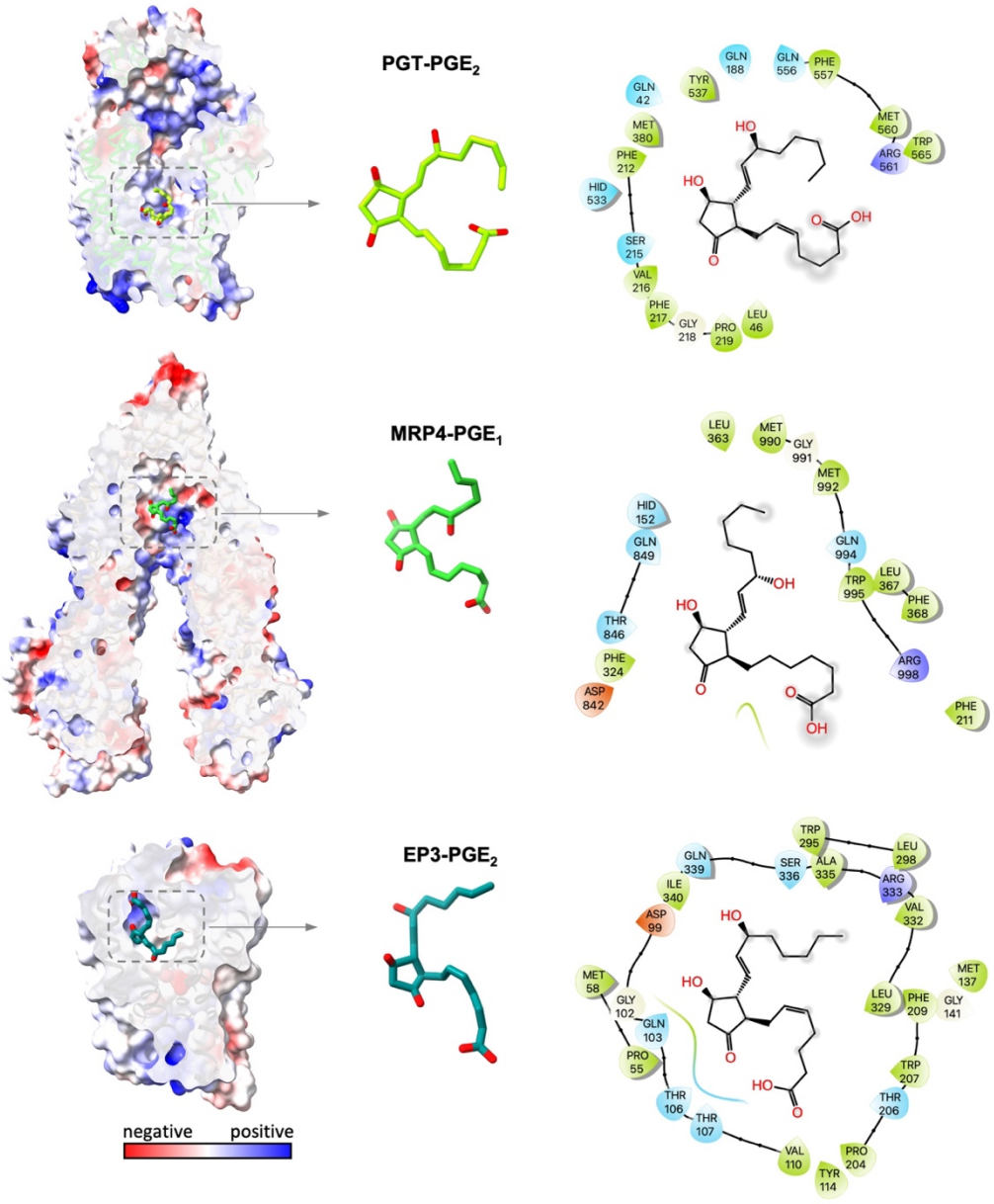

Supplementary Figure 10. L-shape PGEs occupy similar composite pockets of PGT, MRP4 and EP3. The general pattern of PGs interacting with PGT (this study), the PGs exporter MRP4 (PDB: 8IZ9), and receptor EP3 (PDB: 6AK3). The surfaces (left) are colored by electrostatic potential calculated in ChimeraX[49]. The similar compact L-shape PGE_2 molecules (middle) in these complexes are shown as sticks representations. 2D interaction diagram (right) for residues interacting with PGEs, analyzed in Maestro with a distance cutoff of 4.5 Å.

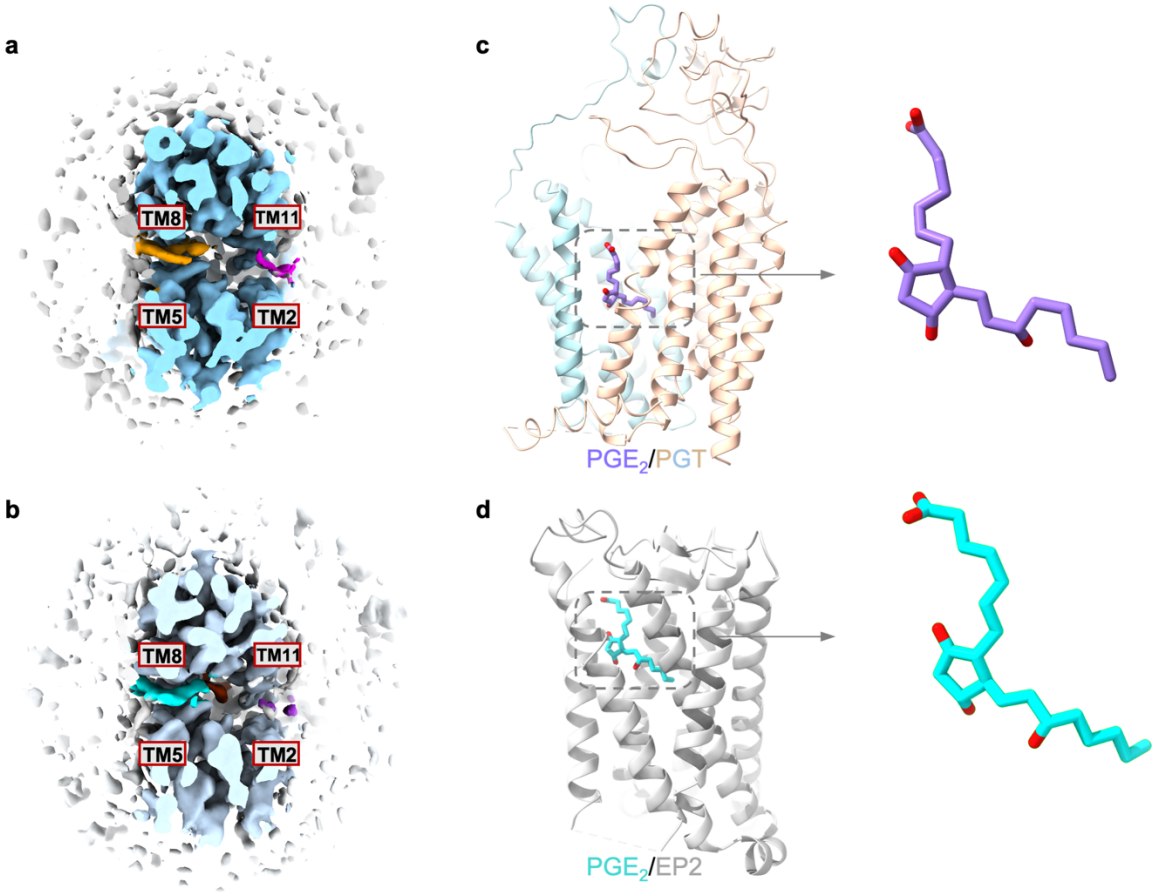

Supplementary Figure 11. Possible elongated PGE_2 pose close to the lateral entry site of PGT. **a** and **b,** Top view of PGT_{apo} (**a**) and PGE_2-bound PGT_{cen} (**b**) cryo-EM maps. Lipid-like densities at extracellular junctions of TM5-TM8 and TM2-TM11 are shown in orange and magenta (**a**), cyan and violet (**b**), respectively. PGE_2 at the central site of transport funnel is colored red (**b**). **c,** The extended conformation of PGE_2 in PGT_{len}. **d,** The extended PGE2 conformation in the EP2-PGE_2 complex structure (PDB: 7CX2).

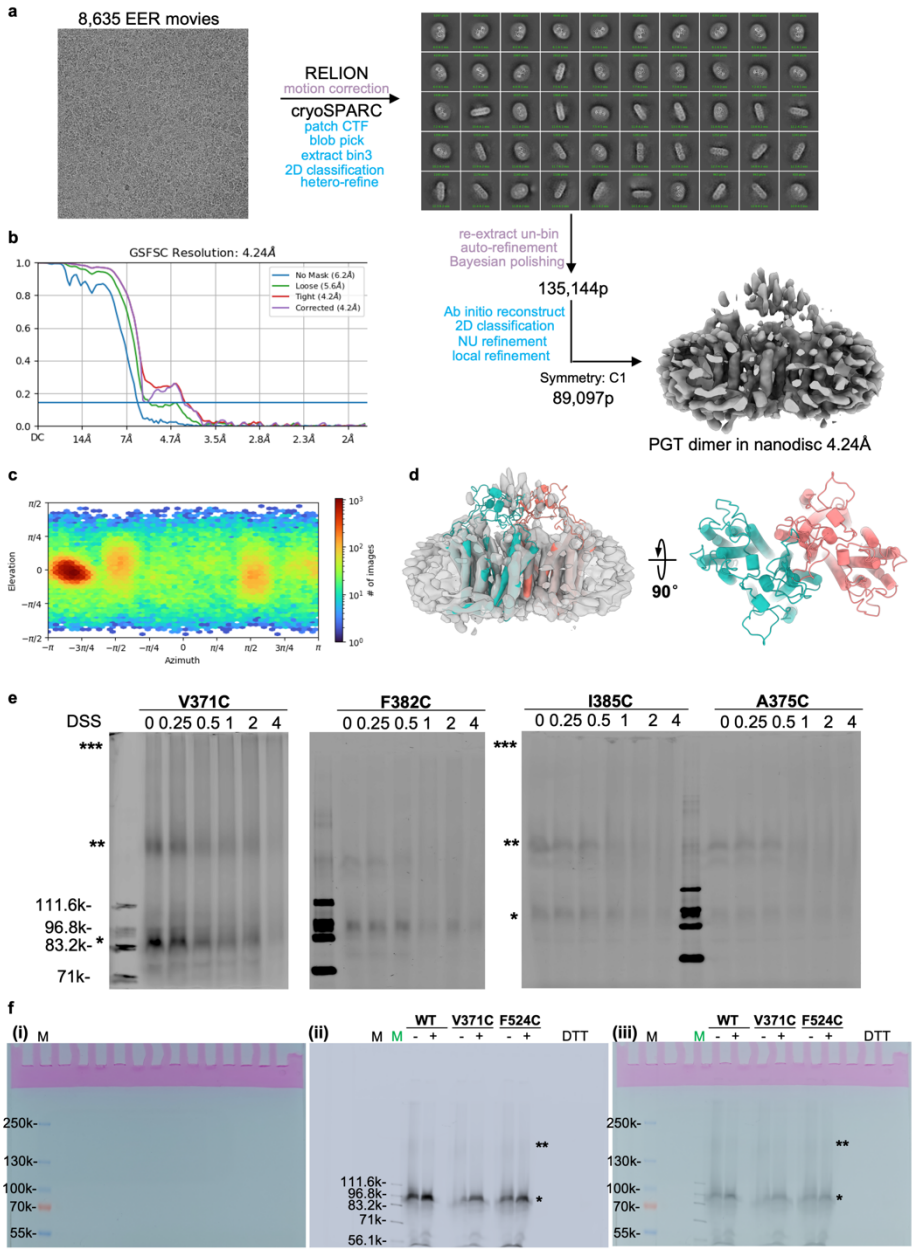

Supplementary Figure 12. Cryo-EM analysis of PGE_2-bound sample in nanodiscs. a, Data processing flowchart for PGE_2/PGT reconstituted in lipid nanodiscs. Representative raw image and 2D class averages are shown on the right. Only discernable dimeric particles are pooled and processed to reconstruct the 4.24-Å PGT map. **b,** Resolution estimated by the gold-standard Fourier shell correlation (GSFSC) with cutoff at 0.143. **c,** Angular distribution heatmap of the final particles in map reconstruction. **d,** The dimeric structural model generated from detergent micelle is docked into PGT/nanodisc map. The ECD region is not well-defined. **e**, DSS crosslinking analysis. eGFP-tagged WT and cysteine substitution mutants were treated with increasing DSS concentrations (0~4 mM), deglycosylated by PNGase F, and visualized by in-gel fluorescence. Oligomeric states (monomer [*] , dimer [**], higher oligomer [***]) were assigned based on molecular size markers derived from in-house prepared GFP-tagged proteins. **f**, Bright field image through a cell-phone (i) and the in-gel fluorescence image taken by Amersham Typhoon 5 scanner (ii). Images were merged on the right (iii). The MW ladders were labelled accordingly.

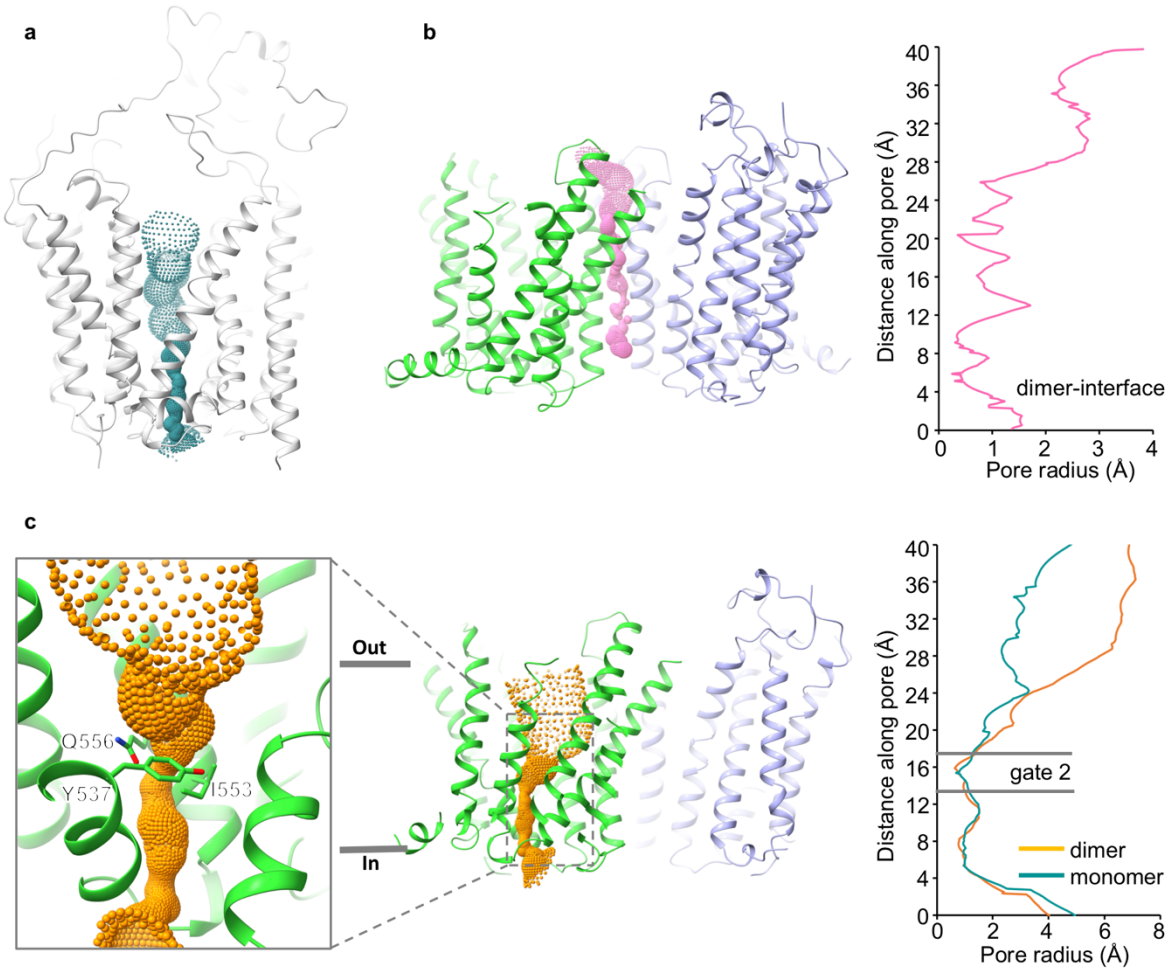

Supplementary Figure 13. Transport funnel changes observed in dimeric PGT_{dd} structure. a, The transport pathway of monomeric PGT_{apo} structure (grey) is plotted by HOLE[62] and represented in blue dots, suggesting the outward-facing conformation. **b,** Overall structure of the PGT_{dd} homodimer. The two protomers are colored in green and blue, respectively. The interface passage is calculated and shown as pink dots. The corresponding radius along the transmembrane axis is plotted on the right. **c,** The expanded transport funnel of PGT_{dd} is analyzed. Residues near the constriction site (gate 2, intracellular side) are shown as stick representations (left). The pore radius (orange, PGT_{dd}; blue, PGT_{apo}) from cytosol to extracellular side is plotted (right).

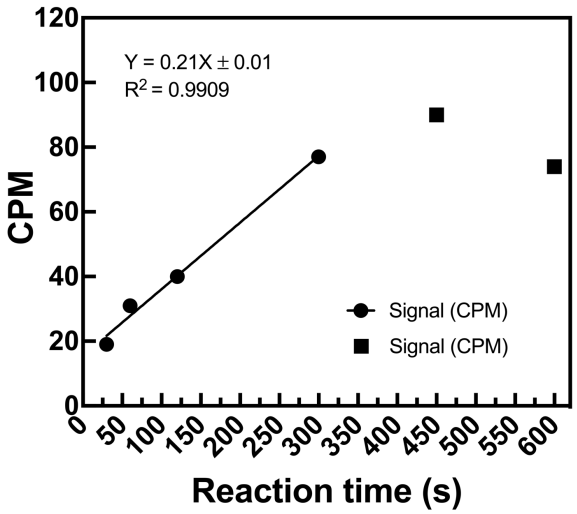

Supplementary Figure 14. A time-course measurement of PGE_2 uptake within 10mins. The data points that in a linear trend were shown as solid circles, while the ones outside the linear trend were depicted as squares.

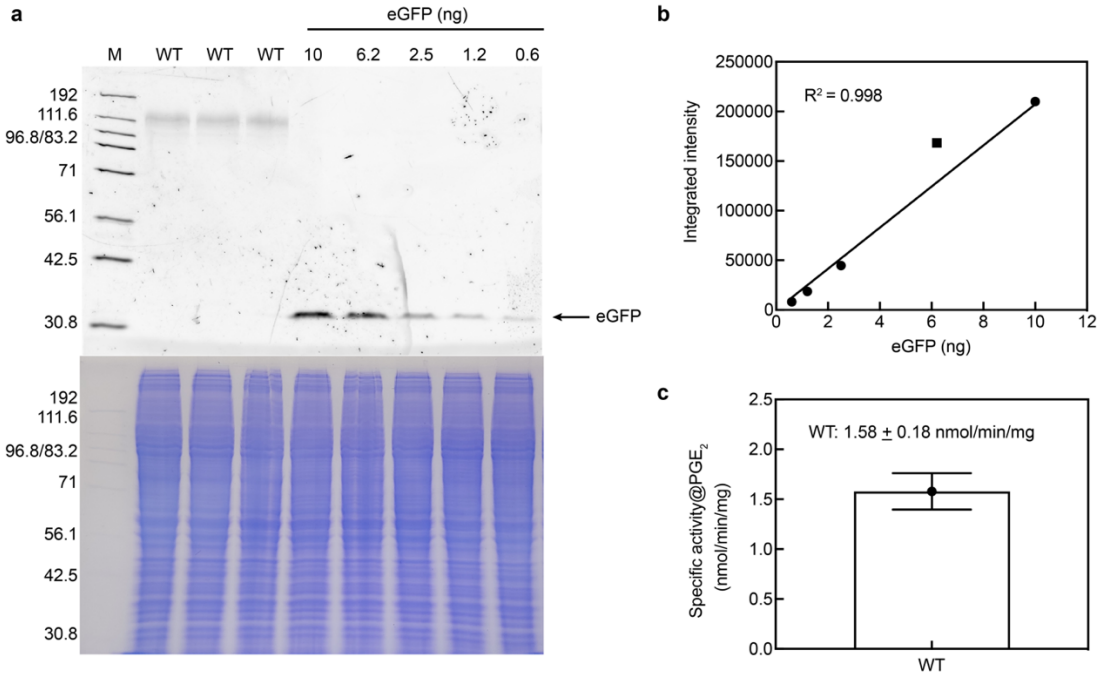

Supplementary Figure 15. Specific activity determination for WT PGT at 80 nM PGE_2 concentration. a, Quantification of the expression level of the eGFP-tagged PGT by in-gel fluorescence (top) using known amounts of free eGFP as calibration standards. The Coomassie staining image of the SDS-PAGE is shown at the bottom. **b,** Linear plot of the integrated band intensity in (**a**) against the amount of eGFP loading. **c,** Specific PGE_2 uptake activity (mean ± SEM, *n*=3 independent expriments) of WT PGT. The amount of PGT (mg) was obtained from the calibration in (**a**) and (**b**).

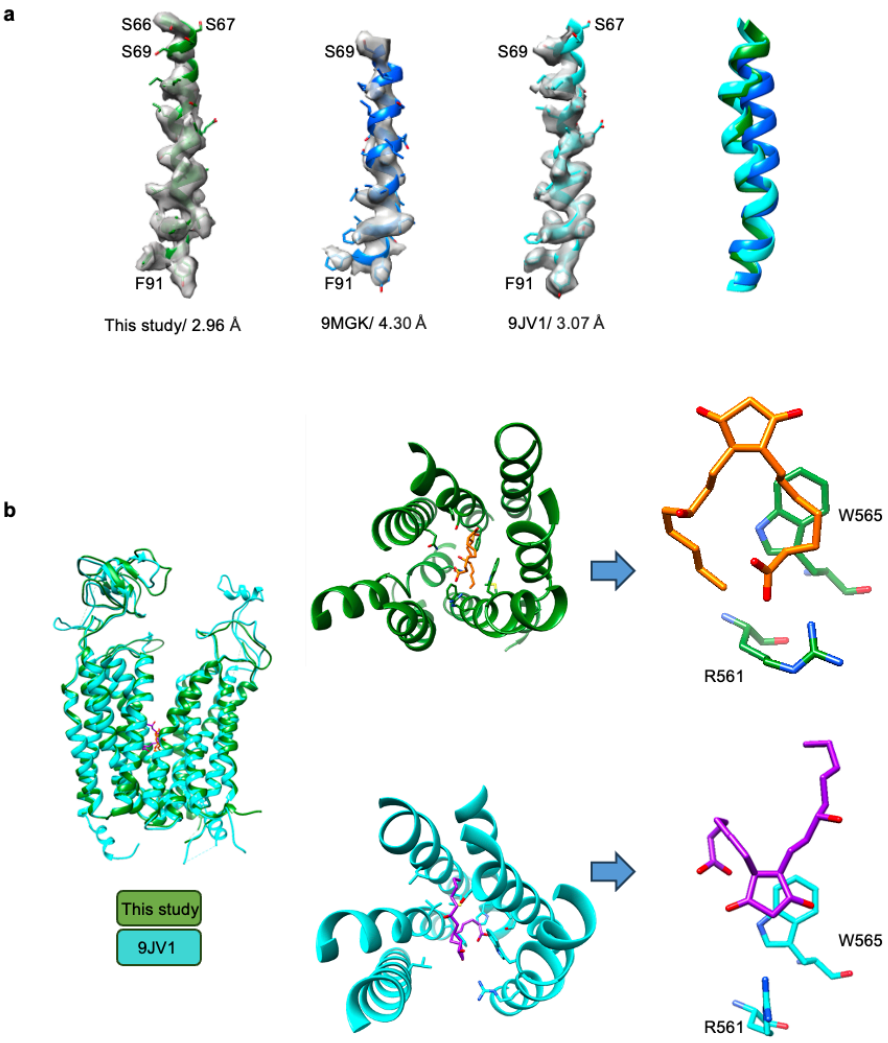

Supplementary Figure 16. Structural comparison of PGT in this study with other reports. a, TM2 conformational diversity in our structure, Orlando group (9MGK) and Jiang group (9JV1). The overlay of 3 structures were shown on right. **b,** Different poses of PGE_2 observed at the central binding site.

	PGT_{apo}	PGT_{cen}	PGT_{len}	PGT_{dd}	PGT_{dn}
Data collection and processing					
Magnification	130,000	130,000	130,000	130,000	130,000
Voltage (kV)	300	300	300	300	300
Electron exposure ($e^-/Å^2$)	50	50	50	50	50
Defocus range (μm)	-1.2 to -2.0	-1.2 to -2.0	-1.2 to -2.0	-1.2 to -2.0	-1.2 to -2.0
Pixel size (Å)	0.932	0.932	0.932	0.932	0.932
Symmetry imposed	C1	C1	C1	C2	C1
Initial particle images (no.)	1,972,183	3,600,339	3,600,339	5,572,522	6,620,881
Final particle images (no.)	278,382	295,880	68,315	101,167	89,097
Map resolution (Å)	3.14	2.96	4.01	3.16	4.24
Refinement					
Initial model used (PDB code)	AlphaFold2 model	8KGV		8KGV	
Map sharpening *B* factor ($Å^2$)	138.9	108.4	192.1	109.4	157.0
Model composition					
non-hydrogen atoms	3,893	4,036		5766	
Protein residues	536	532		782	
Ligands	NAG:1	PGE_2: 1			
B factor ($Å^2$)					
Protein	75.17	75.53		109.40	
Ligand	168.16	51.83			
R.m.s. deviations					
Bond lengths (Å)	0.003	0.003		0.003	
Bond angles (°)	0. 581	0.663		0.668	
Validation					
MolProbity score	1.47	1.49		1.55	
Clash score	8.31	6.08		10.07	
Poor rotamers (%)	0	0		0	
Ramachandran plot					
Favored (%)	97.92	97.14		97.91	
Allowed (%)	2.08	2.86		2.09	
Outliers (%)	0.00	0.00		0.00	
Deposited model (PDB id)	8KGV	8KGW		8KGI	
Deposited map (EMDB id)	37233	37234	37234	37222	37222

Supplementary Table 1. Cryo-EM data collection and refinement statistics.

Systems	Protein conformation	Mutant	pH	No. of POPC	No. of Water	No. of Na+	No. of Cl-	Total atoms	Replicas	Simulation Time (ns)
PGT-apo	Outward	WT	7.4	212	23471	63	79	108087	3	500
PGT-apo	Outward	△135-165	7.4	212	22704	60	74	105268	3	500
PGT-PGE_2-cen	Outward	WT	7.4	211	23266	63	75	106658	4	500
PGT-PGE_2-cen-flip	Outward	WT	7.4	211	23266	63	75	106658	4	500
PGT-PGE_2-cen	Outward	H533F	7.4	210	23300	63	75	106619	4	500
PGT-PGE_2-cen	Outward	H533E	7.4	211	23282	63	74	106730	4	500
PGT-PGE_2-len	Outward	WT	7.4	211	23496	64	80	108073	6	500

Supplementary Table 2. MD system settings.